

Effect of Annealing Treatment Atmosphere on the Structural and Optical Properties of Silver Doped Zinc Oxide Thin Films

Dridi D, Litaïem Y, Karyaoui M, Dimassi W and Chtourou R

Laboratory of Nanomaterials and Systems for Renewable Energies (LaNSER), Research and Technology Center of Energy, Technopôle Borj-Cedria, Hammam-Lif, Tunis, Tunisia

* Corresponding Author

Dridi D, Laboratory of Nanomaterials and Systems for Renewable Energies (LaNSER), Research and Technology Center of Energy, Technopôle Borj-Cedria, Hammam-Lif, Tunis, Tunisia, Tel: 21629483509, Email: donia.dridi88@gmail.com

Citation

Dridi D, Litaïem Y, Karyaoui M, Dimassi W and Chtourou R (2022) Effect of Annealing Treatment Atmosphere on the Structural and Optical Properties of Silver Doped Zinc Oxide Thin Films. J Chem Reac Catal Res 1: 1-16

Publication Dates

Received date: May 31, 2022

Accepted date: July 27, 2022

Published date: July 29, 2022

Abstract

In this work, the effect of annealing atmosphere on structural and optical properties of silver-doped ZnO thin films (SZO) have been investigated. Silver-doped zinc oxide thin films (SZO) deposited onto glass substrates are synthesized using sol-gel technique via spin coating. XRD analysis reveals that the Ag incorporation leads to a decrease in grain size in ZnO: Ag thin films annealed in air and under nitrogen atmospheres. Conversely, an increase in grain size was noticed for Ag doped ZnO thin films annealed under oxygen flow. All films are highly transparent in the visible region for different annealing treatment environment. In addition, band gap energies were found to decrease after Ag doping as compared to those of pure ZnO thin films post-annealed in different atmospheres. As compared to pure ZnO thin films, an increase of the photoluminescence intensity was noticed.

Keywords: ZnO thin films, Sol-gel, Annealing Treatment Atmosphere, Silver-Doping

Introduction

Zinc oxide (ZnO) is an important II-VI group semiconductor and usually adopts an hexagonal wurtzite crystal structure [1-4]. It has distinct advantages over other competitors (ITO, SnO₂) such as abundance in earth crust, non-toxicity, low material costs, chemical stability, a large melting point of 1975°, large excitation binding energy (about 60 meV at room temperature), high lattice constant, high transparency in the visible and near infrared spectral region, a wide range resistivity, and high electron Hall mobility ($200 \text{ cm}^2 \text{Vs}^{-1}$) [1,3,5]. It is a direct wide band gap semiconductor ($E_g = 3.37 \text{ eV}$ at 300 K, n type) [2-7] and from this direct wide band-gap comes a wide interest in its prospects in optoelectronic applications.

Owing to these exclusive properties, ZnO has been considered as one of the strongest candidates in a variety of applications such as optics, mechanics and biomedical sensing nanodevices, gas and chemical sensors, transducers, transparent electrodes in solar cells, photocatalysis, UV photoconductive detectors, UV lasing and short-wavelength optoelectronic devices [8-17].

It is well known that undoped ZnO films show n-type conductivity because of their inherent defects such as oxygen vacancies which act as a donor. The physical properties of ZnO thin films are closely connected with deposition methods, deposition parameters, annealing treatments and doping. Among these factors, the doping has been widely used to adjust the structural, electrical, optical and ferro-magnetic properties. The greatest challenge that needs to be overcome for the realization of the most ZnO based applications is the fabrication of reliable and stable p-type material. P-type ZnO may be achieved by the substitution of group-IA element (Li, Na, and K) [18-20] and group-IB elements such as Cu and Ag [21-23] on the Zn-site, and group-VA elements (N, P, As, and Sb) on the O-site [24, 25], respectively. Among the used doped elements, silver is one of the most promising metal to enhance structural, morphological and optoelectronic properties of ZnO. To date, Ag-doped ZnO thin films have been widely explored for potential applications including photocatalysis [26-28], Dye-sensitized Solar Cells [29] as well as photoelectrode in Photoelectrochemical water splitting solar cells [13,30-31].

In order to prepare Ag-doped ZnO thin films, several deposition techniques have been applied such as, RF magnetron sputtering [32], atomic layer deposition (ALD) [33], e-beam evaporation techniques [34], electrochemical deposition [35], pulse laser deposition (PLD) [36] and sol-gel method [37-39]. Among these

different techniques, sol-gel method attracts much attention not only because it is easier to implement and is generally carried out at near room temperature but also because this technique should be promising for doping ZnO nanostructures since it consists of mixing beforehand dopant sources with zinc atoms precursors. In addition, the preparation of thin films by this method minimizes intrinsic defects and gives good optical quality samples. To best of our knowledge, the effect of annealing treatment atmosphere on physical properties of Ag doped ZnO thin films prepared by sol-gel method has not been reported earlier.

In this paper, undoped and Ag doped ZnO thin films were deposited onto glass substrates by sol-gel technique via spin coating. Then we have investigated the effect of annealing treatment atmosphere on structural and optical properties of SZO thin films.

Experimental Details

Films preparation

Undoped and Ag doped ZnO (SZO) thin films were deposited onto glass substrates by sol-gel technique via spin coating. Before the fabrication process, the substrates were properly cleaned in an ultrasonic cleaner using acetone and ethanol for eliminating any dust or contaminants, then rinsed with distilled water. The precursor solutions were prepared as follows: zinc acetate dihydrate ($\text{Zn}(\text{CH}_3\text{COO})_2 \cdot 2\text{H}_2\text{O}$, 99.9%, Merck), and silver nitrate ($\text{Ag}(\text{NO}_3)$) were used as starting materials, absolute ethanol as solvent and monoethanolamine ($\text{NH}_2\text{CH}_2\text{CH}_2\text{-OH}$, Sigma Aldrich) as a stabilizer. The molar ratio in the solution was varied to give a ratio of [Ag/Zn] ranging from 1% to 3%. The resultant solutions were stirred at 60°C for 2 h and cooled down at room temperature for 24 h to yield a clear, transparent and homogeneous ZnO aqueous solution. The solutions were then employed in the fabrication of the Ag-doped ZnO films by using a spin coating technique. All films were spin-coated on ITO substrates. Spinning speed was kept at 3000 rpm while spinning time was 30s. After a ZnO sol layer was finished, it was put into a furnace for preheating at 300°C for 10 min to remove the organic solvent. Then, the next layer was deposited. The procedure from spin-coating to preheating was repeated for several times in order to obtain the desired film thickness. At last, in order to get crystallized films, all the samples were annealed at 550°C for 2h in air atmosphere, under nitrogen flow and under oxygen flow in a CVD furnace.

Thin films characterizations

The crystalline properties of undoped and Ag-doped ZnO spin coated thin films were characterized by the X-ray diffractometer (Phillips (PW3719) X'pert materials research) with a Cu K α radiation.

The optical measurements in the UV-Visible range were carried out using a LAMBDA 950 UV/Vis/NIR spectrometer from Perkin Elmer within 200 nm –1400 nm wavelength range.

Photoluminescence measurements were achieved at room temperature using Jobin-Yvon spectrometer with 266nm excitation wavelength laser.

Results and Discussion

Structural properties

The X-ray diffraction (XRD) spectra of ZnO and ZnO:Ag thin films deposited onto glass substrates with different Ag doping contents (1%, 2% and 3% Ag) and annealed under different atmospheres are shown in Figures 1, 2 and 3.

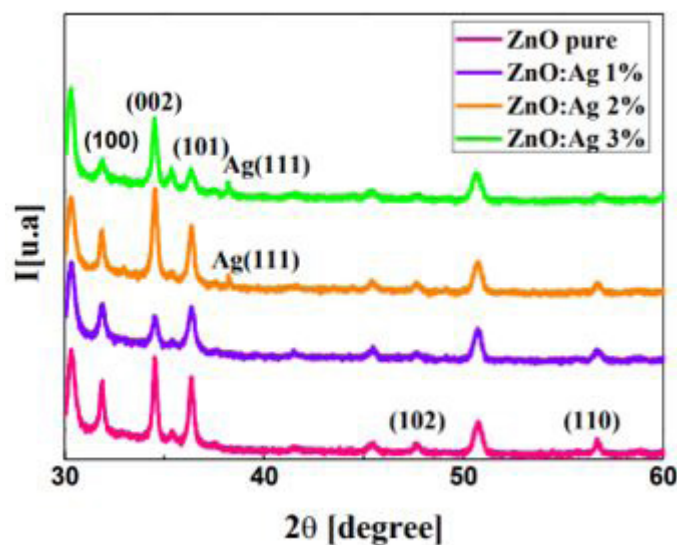


Figure 1: XRD patterns of pure and Ag doped ZnO thin layers deposited onto glass substrates and annealed in air

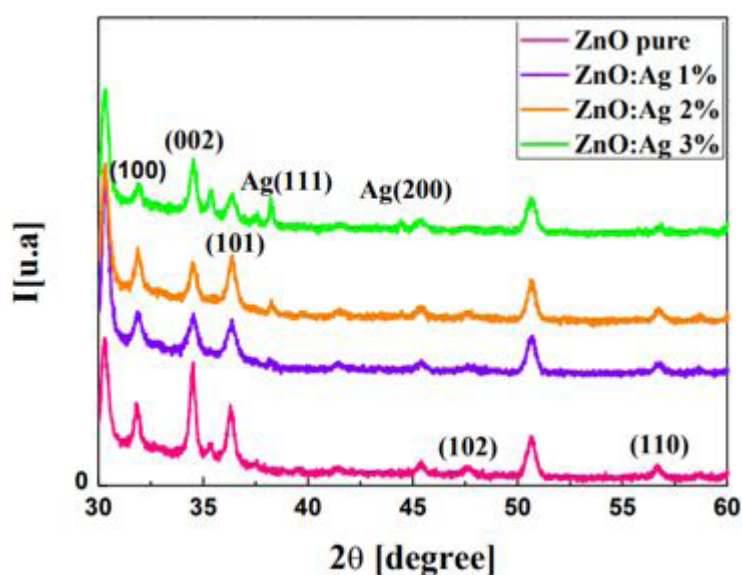


Figure 2: XRD patterns of pure and Ag doped ZnO thin layers deposited on glass substrates and annealed under nitrogen flow

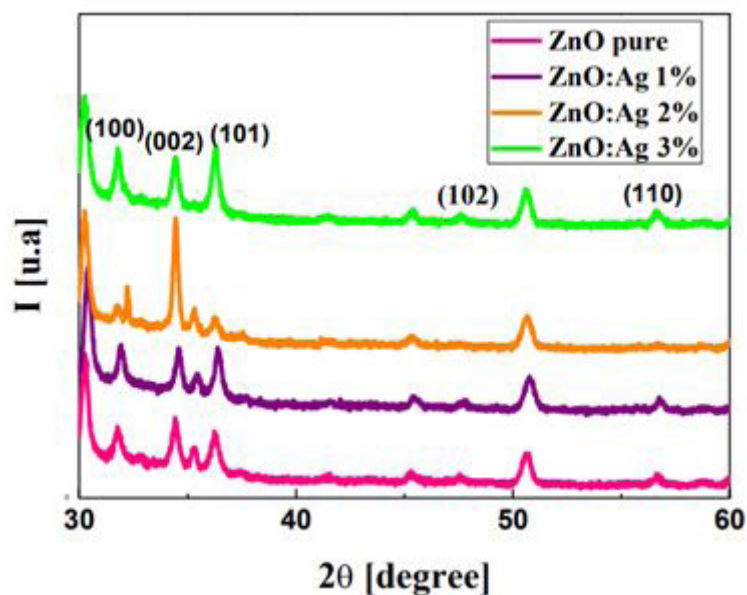


Figure 3: XRD patterns of pure and Ag doped ZnO thin layers deposited on glass substrates and annealed under oxygen flow

The characteristic peak positions for hexagonal würtzite ZnO phase are identified at around 31°, 34°, 36°, 47°, 56° and 62° compared to the standard JCPDS 036-1451 card and its corresponding miller planes are (100), (002), (101), (102), (110) and (103) respectively.

Undoped ZnO thin films show strong peak corresponding to (0 0 2) plane indicating high-c-axis orientation perpendicular to the substrate. We note that this (002) peak intensity has improved with the increase of silver doping content especially for samples annealed in air and under oxygen flow. This trend demonstrates that the crystallinity of the samples was enhanced with the increase in silver doping content from 1% Ag to 3% Ag doping content.

Tables 1-3 illustrate the microstructural parameters evaluated from XRD measurements for ZnO and ZnO:Ag thin films annealed under different annealing treatment atmospheres. It can be seen from Figures 1, 2 and 3 and tables 1-3 that the three major peaks (100), (002) and (101) shift toward higher 2θ values with the increase in Ag doping content and these values are greater than those of the bulk ZnO. This behaviour is against the expectation. However, a decrease in the 2θ peak position value is generally observed when a doping element with a larger ionic radius than Zn^{2+} is replaced at the substitution sites in the ZnO crystal lattice. In fact, several research groups have reported that the shift of (002) peak position towards lower angle [13, 40-44] and attributed this shift to the increase of c-axis lattice constant caused by the substitution of Zn^{2+} ions by Ag^+ ions.

Table 1: The microstructural parameters evaluated from XRD measurements such as, Position peak, lattice spacing (d), lattice parameters (a, c), bond length L, volume of unit cell, grain size (D), micro strain ϵ and density of dislocation δ for ZnO: Ag thin films post annealed in air atmosphere

	Results JCPDS (pure powder ZnO)	Experiment: Ag content Ag/Zn (%)			
		0	1	2	3
2θ (°)					
(002)	34.422	34.464	34.458	34.462	34.448
(101)	36.253	36.288	36.290	36.285	36.279
d_{002} [Å]	2.603	2.600	2.600	2.600	2.601
d_{101} [Å]	2.475	2.473	2.473	2.473	2.4740
a [Å]	3.249	3.246	3.246	3.247	3.2474
c [Å]	5.206	5.2	5.201	5.200	5.202
c/a	1.602	1.601	1.602	1.601	1.602
L [Å]	1.977	1.975	1.975	1.975	1.976

Volume of unit cell	47.6	47.471	47.471	47.483	47.510
D[nm]		44.380	26.559	34.047	31.223
$s (10^{-4})$		26.363	44.060	34.366	37.749
$\delta [lines/m^2] * 10^{14}$		5.077	14.175	8.626	10.257

Table 2: The microstructural parameters evaluated from XRD measurements such as, Position peak, lattice spacing (d), lattice parameters (a, c), bond length L, volume of unit cell, grain size (D), microstrains and density of dislocation δ for ZnO:Ag thin films post annealed under nitrogen flow

	Results JCPDS (pure powder ZnO)	Annealing treatment under nitrogen flow Experiment: Ag content Ag/Zn (%)			
		0	1	2	3
$2\theta (^{\circ})$					
(002)	34.422	34.432	34.459	34.460	34.461
(101)	36.253	36.256	36.2941	36.310	36.307
$d_{002} [\text{\AA}]$	2.603	2.602	2.600	2.600	2.600
$d_{101} [\text{\AA}]$	2.475	2.475	2.473	2.472	2.472
a[\AA]	3.249	3.249	3.246	3.244	3.244
c[\AA]	5.206	5.204	5.200	5.200	5.200
c/a	1.602	1.601	1.602	1.603	1.602
L	1.977	1.977	1.975	1.974	1.974
Volume of unit cell	47.62	47.595	47.458	47.406	47.416
D[nm]		29.359	21.135	24.338	25.533
$s (10^{-4})$		39.887	54.873	48.079	45.829
$\delta [lines/m^2] * 10^{14}$		11.601	22.385	16.881	15.338

Table 3: The microstructural parameters evaluated from XRD measurements such as, Position peak, lattice spacing (d), lattice parameters (a, c), bond length L, volume of unit cell, grain size (D), microstrain s and density of dislocation δ for ZnO:Ag thin films post annealed under Oxygen flow

	Results JCPDS (pure powder ZnO)	Annealing treatment under Oxygen flow Experiment: Ag content Ag/Zn (%)			
		0	1	2	3
$2\theta (^{\circ})$					
(002)	34.422	34.448	34.602	34.467	34.454
(101)	36.253	36.281	36.426	36.305	36.289
$d_{002} [\text{\AA}]$	2.603	2.601	2.59	2.599	2.600
$d_{101} [\text{\AA}]$	2.475	2.473	2.464	2.472	2.473
a[\AA]	3.249	3.247	3.235	3.245	3.246
c[\AA]	5.206	5.202	5.18	5.199	5.201
c/a	1.602	1.602	1.601	1.602	1.602
L[\AA]	1.977	1.976	1.968	1.974	1.975
Volume of unit cell	47.62	47.505	46.952	47.418	47.477
D[nm]		27.635	23.824	37.859	30.671
$s (10^{-4})$		42.357	48.919	30.902	38.158
$\delta [lines/m^2] * 10^{14}$		13.094	17.617	6.976	10.630

The opposite behaviour marked with the shift towards higher 2θ angle confirms that more of Ag^+ ions are either settling into interstitial sites or making clusters. The same trend was also reported by tripathi et al [45] and karki et al [46].

As depicted in figures 1 and 2, we notice the presence of additional peaks at around 38° attributed to the body-centred-cubic phase of metallic Ag (111) according to JCPDS card N° 01-089-3722. The appearance of Ag peak in the diffraction patterns of SZO thin films annealed in air and under nitrogen flow, clearly indicates the formation of crystalline silver clusters in the films.

From tables 1,2 and 3 there is a decrease in terms of lattice constants (a and c) and in the volume of unit cell of Ag doped ZnO films annealed under different atmospheres as compared to those in bulk ZnO.

In case of SZO films annealed in air and under nitrogen flow, the shift of 2θ peak position angles towards higher values and the decrease in lattice constants (a and c) along with the appearance of Ag peak in XRD patterns lead us to conclude that Ag ions are preferably making clusters in Ag doped ZnO films instead of settling in interstitial sites. Conversely, the absence of Ag peaks in XRD patterns for SZO films annealed under oxygen flow along with the shift of 2θ towards higher angles and the decrease in lattice constants may indicate the fact that Ag ions are settling in interstitial sites instead of making clusters in SZO films.

To reach some valuable informations regarding the enhancement of ZnO thin films structure, some calculations have been done. Indeed, the interplanar spacing d_{hkl} values of undoped ZnO ZnO: Ag thin films were also calculated by using Bragg equation (Eq.1) [47] as follows and listed in tables 1, 2 and 3:

$$2d_{hkl} \sin\theta = n\lambda \quad (1)$$

In the same way, by using the relationship of d_{hkl} for the hexagonal system and inclusion of miller indices for the planes (002) and (101), we have deduced the appropriate lattice constants a and c [48] as follows using (Eqs. 2, 3 and 4);

$$\frac{1}{d_{hkl}^2} = \frac{4}{3} \left[\frac{h^2 + hk + k^2}{a^2} \right] + \frac{l^2}{c^2} \quad (2)$$

$$c = 2 d_{002} \quad (3)$$

$$a = \frac{2cd_{101}}{\sqrt{3(c^2 - d_{101}^2)}} \quad (4)$$

The volume (V) of the unit cell for ZnO wurtzite hexagonal system has been calculated using the following formula (Eq.5):

$$V = 0.866 * c * a^2 \quad (5)$$

It was found that the volume of unit cell decreases with increasing Ag content. It may be due to decreasing the lattice parameters 'a' and 'c'. When Ag atoms are introduced, there is a change in the electronic bonding between the nearest two atoms which affect the Zn-O bond length. The Zn-O bond length (L) is calculated [49] using the following formula (Eq. 6):

$$L_{\text{Zn-O}} = \sqrt{\frac{a^2}{3} + \left(\frac{1}{2} - \frac{c}{2}\right)^2} \quad (6)$$

With

$$= \frac{a^2}{3c^2} + 0.25 \quad (7)$$

The variations in lattice parameters, unit cell volume, crystallite size, bond length of $\text{Zn}_{1-x}\text{Ag}_x\text{O}$ thin films, microstrain and density of dislocations are reported in Tables 1.2 and 3. From the tables,

it is clear that as Ag doping contents increase in SZO thin films annealed under different environment, the lattice constants (a and c), the volume of unit cell and the Zn-O bond length have decreased consequently.

On the other hand, the grain size D values are estimated from (002) diffraction peaks of all SZO thin films, using Debye-Scherrer formula (Eq. 8) [50];

$$D = \frac{k\lambda}{Q_{1/2} \cos\theta} \quad (8)$$

Where $\lambda = 0.15405$ nm is the wavelength of Cu K α radiation, $Q_{1/2}$, the full width at half maximum (FWHM) of the main diffraction peak in radian, θ , the Bragg angle and K, the Scherrer's constant (equal to 0.90 according to the widespread practical).

The evolution of grain size vs various Ag doping concentration and under different annealing treatments environment is illustrated in Figure 4. As compared to undoped ZnO, the grain sizes of SZO thin films decrease slightly with the increase in Ag doping content noticed especially for films annealed in air and under nitrogen flow. This is in good agreement with the reported result of Liu et al [51], they found that the Ag-doping led to a smaller ZnO grains. However, the grain size of SZO films annealed

under oxygen flow has been slightly decreased from 27.63 nm for undoped ZnO to 23.82 nm with low doping concentration 1% and increases with further increase in Ag doping concentration reaching a maximum grain size value around 37.85 nm for 2% Ag doping content.

The microstrain (ξ), which is an interesting structural parameter of ZnO:Ag spin coated thin films is calculated using the following relation (Eq.9) [52]:

$$\xi = \frac{Q_{1/2}}{4 \tan \theta} \quad (9)$$

where, $Q_{1/2}$ is the full-width at half-maximum of (002) peak and θ is the Bragg angle. The evolution of microstrain vs various Ag doping concentration and under different annealing treatment atmospheres was shown in Figure 5. As illustrated in tables 1, 2 and 3 and Figure 5, the strain values decrease with increasing Ag doping concentrations.

The number of dislocations in a material is defined as the dislocation density (δ) which represents the amount of defects in a film. It has been defined as the length of dislocation lines per unit volume or the number of dislocations intersecting a unit area which can be estimated as (Eq. 10)[53];

$$\delta = \frac{n}{D^2} \quad (10)$$

where n is a factor which is equal to unity giving minimum dislocation density and D is crystallite size.

From this structural study, we point out the fact that the decrease in grain size (D) as well as the increase of both of the strain and the dislocation density are indeed understood as an important role played by the introduction of Ag doping element

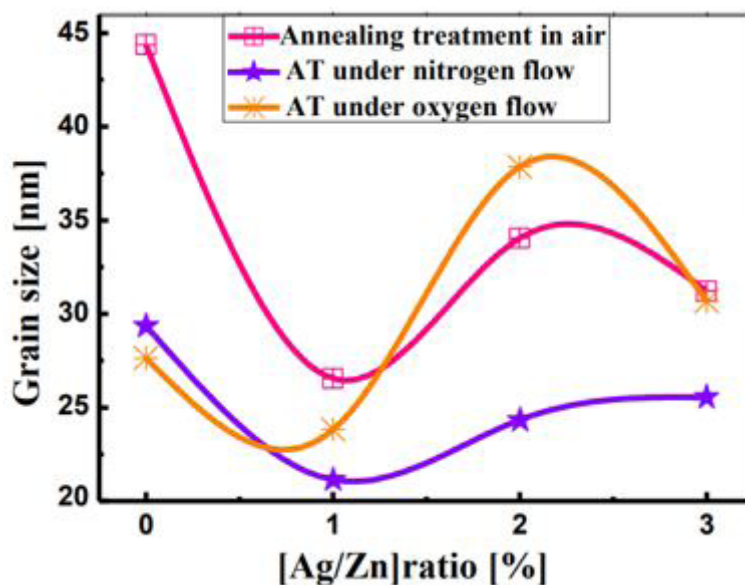


Figure 4: Variation of the grain size with various Ag doping concentrations for thin films post annealed under different environment of annealing treatments

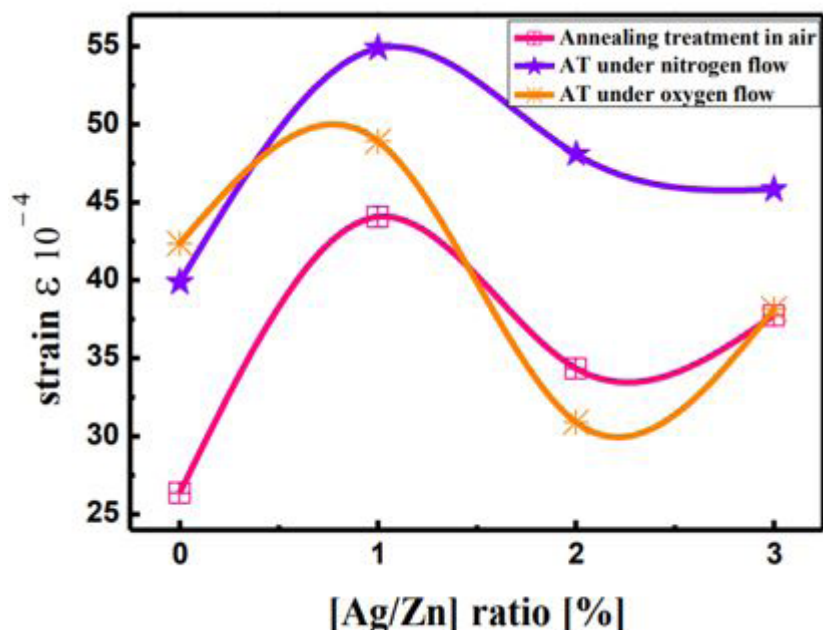


Figure 5: Variation of the strain in ZnO and ZnO:Ag films annealed under different environments of annealing treatments

Optical Properties

UV- Vis measurements

Transmittance plots of undoped and Ag-doped ZnO (SZO) films deposited onto glass substrates after annealing treatments in air, under nitrogen flow and under oxygen flow are shown in Figures 6,7 and 8.

Undoped ZnO thin films exhibit high transparency in the visible region. The transmittance of all SZO films in the visible region (400 nm-800 nm) is about:

- 70% - 80% for SZO films annealed in air.
- 75% - 80% for SZO films annealed under nitrogen flow.
- 80% - 85% for SZO films annealed under oxygen flow.

It can be seen that the drastic decrease in transmittance corresponds to a sharp absorption edge in the near-UV region (NBE). Also, we can notice the presence of interference fringes which can be attributed to reflections on the surface of the layer at the interface layer/substrate.

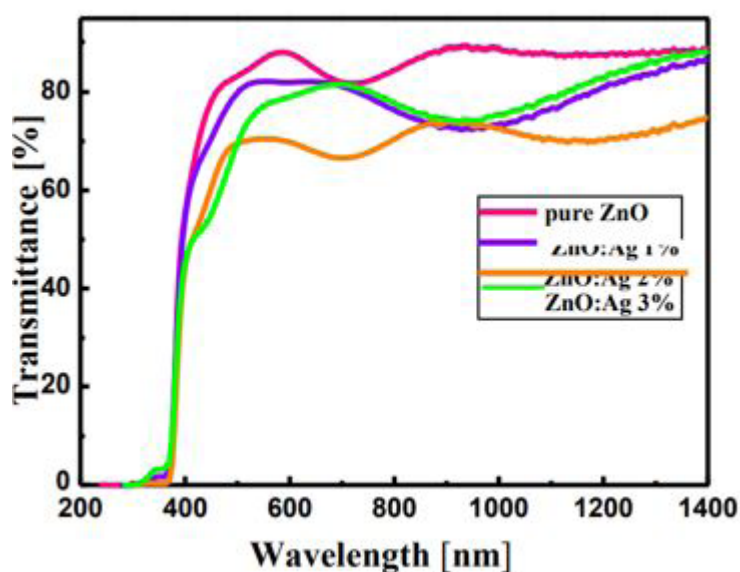


Figure 6: Transmittance spectra of SZO thin films annealed in air

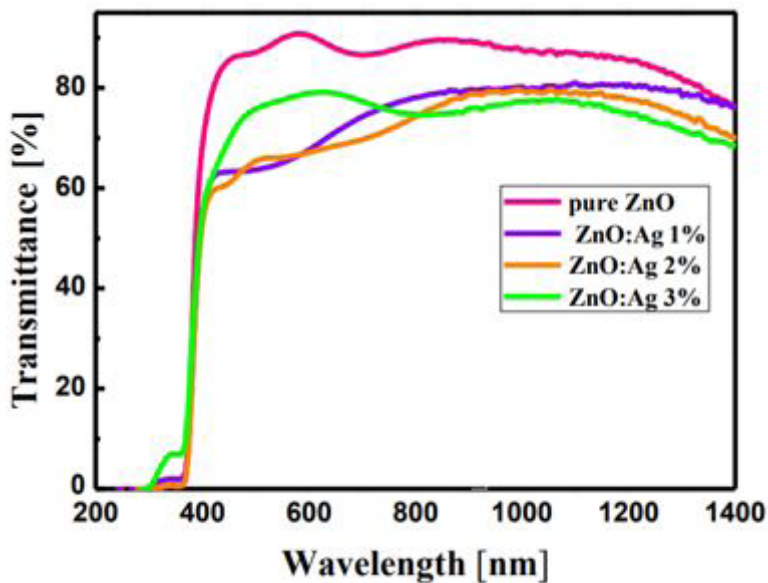


Figure 7: Transmittance spectra of Silver-doped ZnO thin films annealed under nitrogen flow

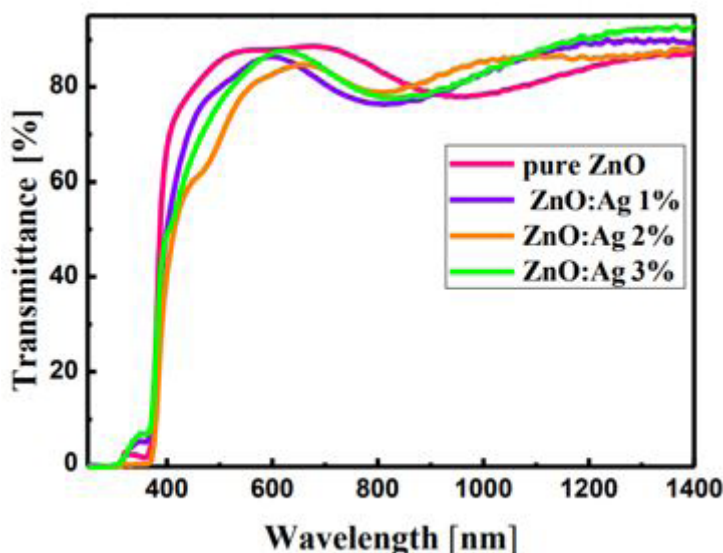


Figure 8: Transmittance spectra of silver-doped ZnO thin films post-annealed under oxygen flow

The fundamental absorption edge of the films corresponds to transitions of electrons from the valence band to the conduction band edge and this can be used to calculate the difference in the optical band gap of the films. In order to calculate the optical band-gap energy (E_g) of SZO thinfilms, the absorption coefficient can be estimated as (Eq.11) [54]:

$$a = \frac{1}{d} \ln \left[\frac{(1-R)^2}{T} \right] \tag{11}$$

Where T and R are the transmittance and reflectance coefficients respectively and d is the film thickness.

For the direct band gap of the ZnO Würtzite structure, its absorption coefficient and band gap obey to the following relationship (Eq.12) [55]:

$$a h\nu = A (h\nu - E_g)^{\frac{1}{2}} \tag{12}$$

Where A is a constant, $h\nu$ is the photon energy and E_g is the optical band gap.

If one plots $(\alpha h\nu)^2$ vs. photon energy $h\nu$, optical band gap (E_g) of ZnO and Ag-doped ZnO thin films can be obtained

by extrapolating the linear part of the curve to $(\alpha h\nu)^2 = 0$. The related curves for our SZO samples are shown in Figures 9, 10 and 11 and The calculated values of optical band gap (E_g) of Ag-doped ZnO thin films annealed under different atmospheres are summarized in Table 4 and depicted in figure 12.

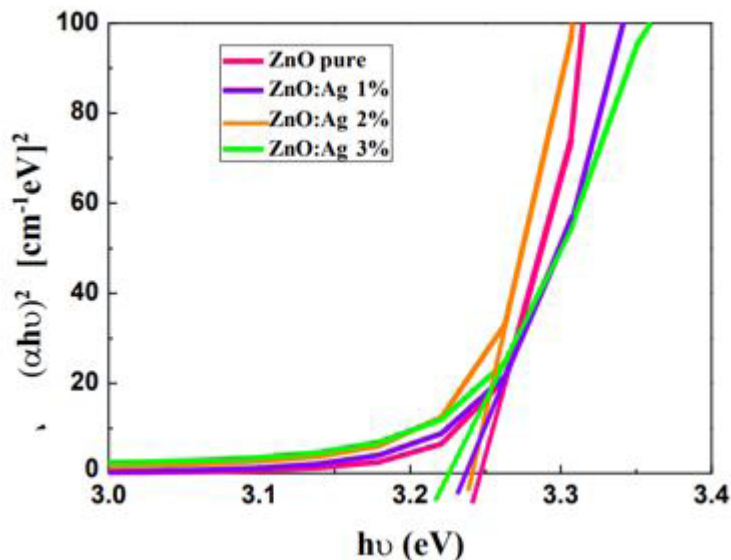


Figure 9: Plots of $(\alpha h\nu)^2$ vs. photon energy $h\nu$ of Ag-doped ZnO thin films annealed in air

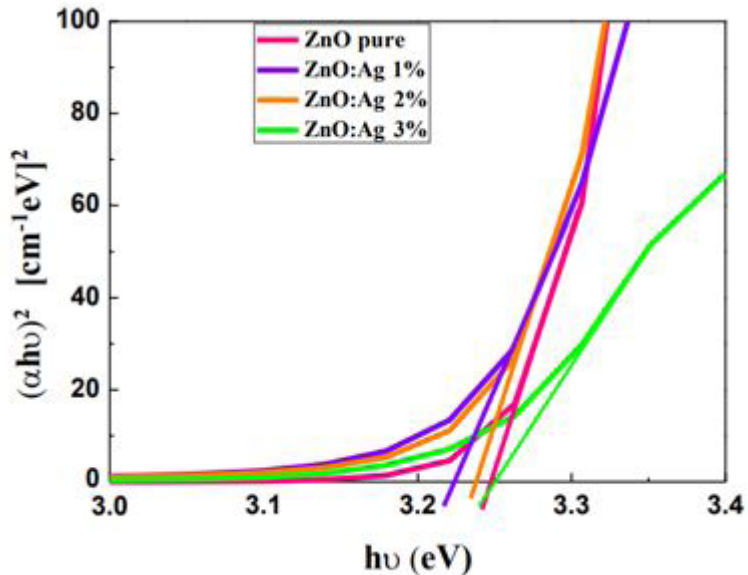


Figure 10: Plots of $(\alpha h\nu)^2$ vs. photon energy $h\nu$ of silver-doped ZnO thin films annealed under nitrogen flow

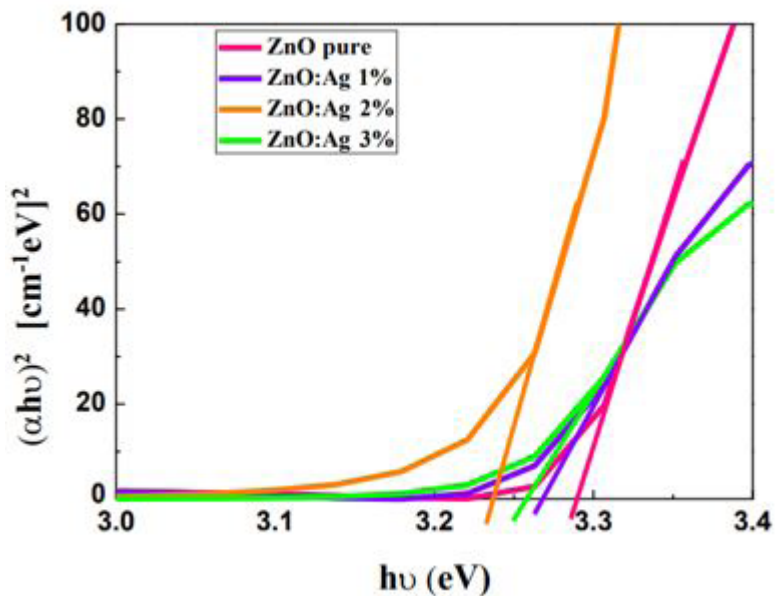


Figure 11: Plots of $(\alpha h\nu)^2$ vs. photon energy $h\nu$ of silver-doped ZnO thin films annealed under oxygen flow

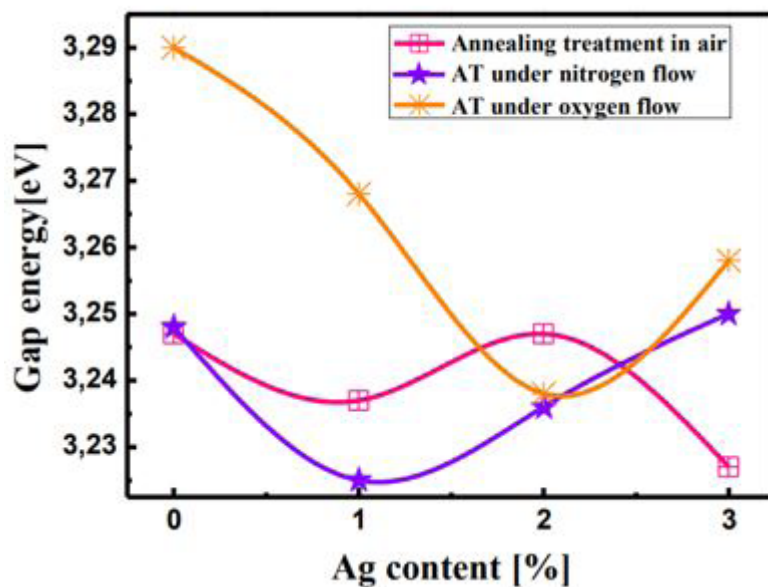


Figure 12: Plots of gap energy vs various Ag doping concentrations annealed under different atmospheres

Table 4: Values of optical band gap of silver-doped ZnO thin films under different heating treatment conditions

		Silver doping %			
		0	1	2	3
E_g (eV)	Annealing treatment in air	3.247	3.237	3.242	3.225
	Annealing treatment under nitrogen flow	3.248	3.225	3.236	3.25
	Annealing treatment under oxygen flow	3.29	3.268	3.238	3.258

The optical band gaps of undoped ZnO annealed in air and under nitrogen flow fall in the same range at about 3.24 eV. Whereas, the optical band gap of pure ZnO thin film annealed under oxygen flow was found around 3.29 eV. Silver incorporation leads to an obvious decrease in SZOband gaps annealed in these three different atmospheres. In fact, the minimum band gap values were obtained with 3% Ag doping content for SZO films annealed in air (3.22 eV), with low doping content 1% Ag for SZO films annealed under nitrogen flow (3.22 eV) and with 2% Ag doping concentration in case of SZO films annealed under oxygen flow (3.23 eV). The decrease of band gap energy after the incorporation of Ag into SZO thin films annealed under different atmospheres may be attributed to the segregation of Ag atoms to

grain boundaries. In fact, these atoms of silver have introduced electron localized states at the ZnO band-gap closer to the lower edge of conduction band forming new lowest unoccupied molecular orbital, which leads in the band gap reduction. The decrease of the band gap with increasing Ag doping in ZnO has been also revealed in several previous reported results [56,57].

Photoluminescence studies

As the exciton binding energy of ZnO is quite high at RT, exciton emission in UV region is possible in ZnO thin films. The photoluminescence spectra of undoped ZnO and Ag-doped ZnO thin films annealed under different atmospheres are recorded at room temperature and shown in Figures 13-15.

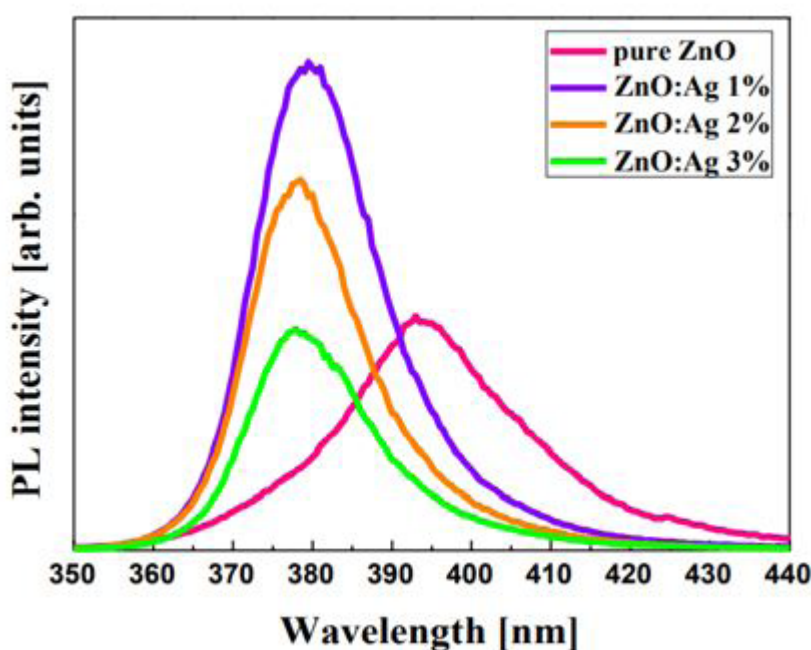


Figure 13: Photoluminescence spectra of ZnO:Ag thin films vs wavelength annealed in air atmosphere

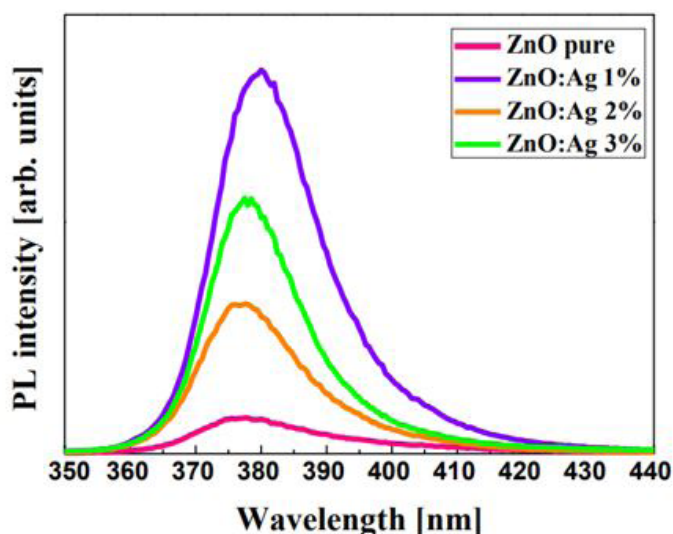


Figure 14: Photoluminescence spectra of ZnO:Ag thin films vs wavelength annealed under nitrogen flow

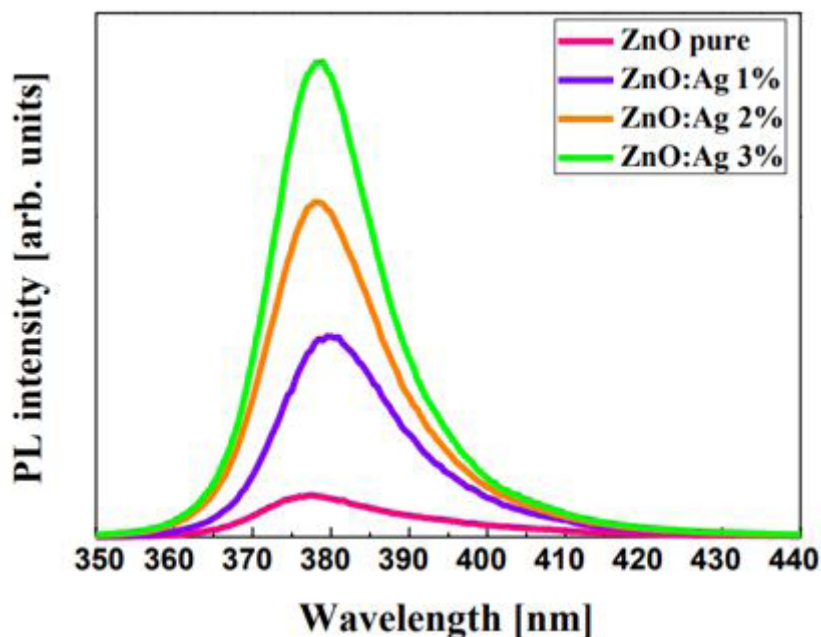


Figure 15: Photoluminescence spectra of ZnO: Ag thin films vs photon energy annealed under oxygen flow

A weak violet peak was observed for undoped ZnO films located at about 394.7 nm for films annealed in air, at around 379.82 nm for ZnO thin film annealed under nitrogen flow and at about 377.64 nm for ZnO film annealed under oxygen flow. In literature, there is a consensus that the UV emission of ZnO belongs to the near band edge emission (NBE) since its position is located close to the band gap energy (~ 3.3 eV) of ZnO at room temperature [58] and it was attributed to the radiative recombination of free excitons [39]. However, this UV peak was downshifted to about 377.64 nm for 3% Ag content after silver doping into SZO thin films annealed in air. In addition, this UV peak for SZO films annealed under nitrogen flow was down shifted to about 378.043 nm for 3% Ag doping content. The same trend was also observed with Xue et al [59] in their study concerning the influence of Ag doping on the optical properties of ZnO films.

In case of SZO thin films annealed under oxygen flow, there is a slight shift toward higher UV peak position after Ag doping

The intensity of this UV peak for SZO annealed in air atmosphere has increased as the Ag concentration in the films increased to 1% Ag compared to undoped ZnO films and then decreased as the Ag concentration further increased from 2% to 3% Ag.

In case of SZO films annealed under nitrogen flow atmosphere, the Ag incorporation leads to a gradually increase in UV peak as compared to pure ZnO film which has the minimum intensity. The same behavior of enhanced UV peak intensities for SZO thin films annealed under oxygen flow as compared to pure ZnO film. The intensities of the UV peak for all the SZO films annealed under different atmospheres increase as Ag doping concentration increase and this behavior is in well agreement with the result obtained by Akhilesh Tripathi et al [45] in their study concerning the UV enhancement in polycrystalline Ag-doped ZnO films deposited by the sol-gel method

Table 5 exhibited the band gap values measured from UV-Vis Transmittance (opt) and from PL measurements. The gap energies of silver-doped ZnO thin films could be derived from optical measurements. All the estimated values are listed in table 5.

Table 5: Band gap energies estimated from UV-Vis transmittance and from PL measurements and UV peak positions of all SZO films annealed under different atmospheres of annealing treatments

[Ag/Zn] %		$E_g(\text{Opt})[\text{eV}]$	UV peak position [nm]	$E_g(\text{PL}) [\text{eV}]$
Annealing treatment in air	0	3.247	394.708	3.142
	1	3.237	380.739	3.258
	2	3.242	379.261	3.2708
	3	3.225	377.642	3.284
Annealing treatment under nitrogen flow	0	3.248	379.821	3.266
	1	3.225	381.193	3.254
	2	3.236	378.665	3.275
	3	3.25	378.043	3.281
Annealing treatment under oxygen flow	0	3.29	377.642	3.284
	1	3.268	380.37	3.261
	2	3.238	378.043	3.281
	3	3.258	378.445	3.277

Therefore, optical band gap energies estimated from UV-Vis transmittance data were found in the range 3.24 eV - 3.22 eV for SZO thin films annealed in air atmosphere. However, Band gap values estimated from PL spectra were slightly modified and fall in the range 3.25 eV - 3.28 eV except the undoped ZnO thin film that has the minimum value of band gap around 3.14 eV. A clear band gap redshift between (opt) and E_g (PL) was noted for the whole SZO thin films annealed in air atmosphere. This redshift mainly arises from either intrinsic or extrinsic defects in the film which can easily form recombination centers. Thus, these defects introduce levels inside the band gap of semiconductor material.

The same trend of band gap redshift between (opt) and E_g (PL) was noted for the whole SZO thin films annealed in both of annealing treatment atmospheres either under nitrogen flow or under oxygen flow.

Conclusion

Silver-doped ZnO thin films have been successfully prepared using sol-gel method onto glass-coated glass substrates. The effect of Ag doping content (1, 2 and 3%) on structural and optical properties was investigated. As compared to undoped, it was found that Ag doping leads to a decrease in grain size and band gap values for both of air and nitrogen post-annealing treatment. However, for oxygen post-annealing atmosphere grain size was found to increase after Ag incorporation allowed by a decrease in band gap. All films are highly transparent in the visible region

for different annealing environment. In addition, band gap energies were found to decrease after Ag doping as compared to those of pure ZnO thin films post-annealed in different atmospheres. As compared to pure ZnO thin films, an increase of the photoluminescence intensity was observed.

Acknowledgements

This work was supported by the Ministry of Higher Education and Scientific Research of Tunisia.

References

1. Ellmer K, Klein A, Rech B (2008) Eds, Springer-Verlag: Berlin Heidelberg Germany. 104: 1-3,
2. Bundesmann C, Schmidt-Grund R, Schubert M. In *Transparent Conductive Zinc Oxide—Basics and Applications in Thin Film Solar Cells* Springer Series in Materials Science.
3. Chen JL, Chen D, Chen ZH (2009) Optimization of the process for preparing Al-doped ZnO thin films by sol-gel method. *Sci China Ser E Tech Sci* 52: 88-94,
4. Tseng YK, Gao GJ, Chien SC (2010) *Thin Solid Films* 518: 6259-6263.
5. Pearton SJ, Norton DP, Ip K, Heo YW, Steiner T, Vac J (2004) *Sci Technol B* 22: 932-948.
6. Lupan O, Shishiyanu S, Ursaki V, Khallaf H, Chow L, et al. (2009) *Sol Energy Mater Sol Cells* 93: 1417-1422.
7. Von Wenckstern H, Schmidt H, Brandt M, Lajn A, Pickenhain R, et al. (2009) *Prog Solid State Chem* 37: 153-172.
8. Znaidi LT, Touam D, Vrel N, Souded S, Ben Yahia O, et al. (2013) *Boudrioua Coatings* 3: 126.
9. Gurav KV, Gang MG, Shin UM, Patil PR, Deshmukh GL, et al. (2014) *ctuators B: Chem* 190: 439.
10. L, Tang S, Yang Z, Wang B (2013) *Zhou Ceram Int* 39: 5771-5776.
11. Shinde SS, Bhosale CH, Rajpure KH (2013) *Photochem Photobiol. B: Biol* 120: 1.
12. Tarwal NL, Devan RS, Ma YR, Patil RS, Karanjkar MM, Patil PS (2012) *Electrochim Acta* 72: 32.
13. Dridi D, Bouaziz L, Karyaooui M, Litaïem Y, Chtourou R (2018) *J Mater Sci-Mater El* 29: 8267-8278.
14. Thongsuriwong K, Amornpitoksuk P, Suwanbon S (2012) *Sol-Gel Sci Thechnol* 62: 304.
15. Wang T, Wu H, Wang Z, Chen C, Liu C (2012) *Appl Phys Lett* 101: 161.
16. Abdulgafour HI, Hassan Z, Ahmed NM, Yam FK (2012) *J Appl Phys* 112: 074.
17. Zhang H, Shen R, Liang H, Liu Y, Liu Y, et al. (2013) *Phys D Appl Phys* 46: 65.
18. Wanga M, Kim EJ, Hahn Lumin SH (2011) 131: 1428.
19. Wang LW, Wu F, Tian DX, Li WJ, Fang L, et al. (2015) *Zhou Alloy Comp* 623: 367.
20. Xu L, Fang GU, Jing SU, Chen Y, Li X, Wang X (2011) *Alloy, Comp*, 509 2942.
21. Yuan H, Xu M, Huang QZ (2014) *Alloy Comp* 616: 401.
22. Tarwal NL, Gurav KV, Mujawar SH, Sadale SB, Nam KW, et al. (2013) *Ceram Int*.
23. Wang ZL (2012) *Adv Mater* 24: 4632.
24. Singh N, Kumari B, Sharma S, Chaudhary S, Upadhyay Vibha R, et al. (2014) *Energ* 69: 242.
25. Yu S, Zhang W, Li L, Dong H, Xu D, Jin Y (2014) *Appl Surf Sci*.
26. Sutanto H, Wibowo S, Nurhasanah I, Hidayanto E, Hadiyanto H (2016) *Int J Chem Eng*.
27. Sutanto H, Nurhasanah I, Hidayanto E (2015) *Mater Sci Forum* 827: 3-8.
28. Badawy MI, Mahmoud FA, Abdel-Khalek AA, GadAllah TA, Abdel Samad Desalin AA (2014) *Water Treat* 52: 13-15.
29. Lanjewar M, Gohel Inorg JV (2016) *Nano-Metal Chem* 47: 1090-1096.
30. Singh N, Choudhary S, Upadhyay S, Satsangi VR, Dass S, Shrivastav R (2014) *Solid State Electrochem* 18: 523-533.
31. Tarwal NL, Patil PS (2011) *Electrochim Acta* 56: 6510-6516.
32. Li WJ, Kong CY, Ruan HB, Qin GP, Huang GJ, et al. (2012) *Fang Solid State Commun* 152: 147-150.

33. Yung-Chen, Cheng Kai-Yun, Yuan Miin-Jang Chen (2016) *Alloy Comp* 685: 391.
34. Xu L, Zheng G, Wanga J, Xian F, Liu Y (2016) *Optik* 127: 5942-5949.
35. Thomas MA, Sun WW, Cui JB (2012) *Phys, Chem, C* 116: 6383.
36. Lu YM, Li XP, Su SC, Cao PJ, Jia F, et al. (2014) *Zhu Lumin* 152: 254.
37. Xu L, Zheng G, Zhao L, Pei S (2015) *Lumin* 158: 396.
38. Touam T, Boudjouan F, Chelouche A, Khodja S, Dehimi M, et al. (2015) *Boudrioua Optik* 126: 5548.
39. Boudjouan F, Chelouche A, Touam T, Djouadi D, Khodja S, et al. (2015) *Lumin* 158: 32.
40. Lee DH, Park KH, Kim S, Lee SY (2011) *Thin Solid Films* 520 1160.
41. Karunakaran C, Rajeswari V, Gomathisankar P (2011) *Superlattices Microstruct* 50: 234.
42. Jin Y, Cui QY, Wang K, Hao J, Wang Q and Zhang J (2011) *Appl Phys* 109: 053521.
43. Xiang Q, Meng G, Zhang Y, Xu J, Xu P, Pan Sens Q (2010) *Actuator B: Chem* 2: 635.
44. Dridi D, Yousra Litaïem, Karyaoui M and Chtourou R (2019) *Eur Phys J Appl Phys*.
45. Tripathi A, Prakash Misra K, Shukla RK (2014) *Lumin* 149: 361-368.
46. Karki B, Nakarmi JJ, Singh RB, Banerjee M (2018) *Inst Sci Tech* 22: 2469.
47. Bragg WL (1913) *Proceedings of the Cambridge Philosophical Society* 17: 43-57.
48. Peng LP, Fang L, Yang XF, Li YJ, Huang QL, Wu F, et al. (2009) *J Alloys Compd* 484: 575-579.
49. Chand P, Gaur A, Kumar A (2013) *Superlattices Microstruct* 64: 331-342.
50. Tripathi R, Kumar A, Bharti C, Sinha TP (2010) *Curr Appl Phys* 2: 676-681.
51. Liu K, Yang B, Yan H, Fu Z, Wen M, et al. (2008) *Appl Surf Sci* 255: 2052.
52. Sahay PP, Nath RK (2008) *Sens Actuators B* 134: 654-659.
53. Saleem M, Fang L, Wakeel A, Rashad M, Kong CY (2012) *World J Condens Matter Phys* 2: 10-15.
54. Rmili A, Ouachtari F, Bouaoud A, Louardi A, Chtouki T, et al. (2013) *J Alloys Compd* 557: 53-59.
55. Zebbar N, Aida MS, Hafdallah A, Daranfadh W, Lekiket H, Kechouane M (2009) *Mater Sci Forum* 609: 133-137.
56. Karyaoui M, Mhamdi A, Kaouach H, Labidi A, Boukhachem A, et al. (2015) *Mater Sci Semicond Process* 30: 255.
57. Sahu DR (2007) *Microelectron* 38: 1252.
58. Garcia MA, Merino JM, Fernández Pinel E, Quesada A, de la Venta J, et al. (2007) *Hernando Nano Lett* 7: 14-89.
59. Xue H, Xu XL, Chen Y, Zhang GH, Ma SY (2008) *Appl Surf Sci* 255: 1806.